Liquid-vapor phase equilibrium of a simple liquid confined in a random porous media: Second-order Barker-Henderson perturbation theory and scaled particle theory

A. K. Nelson[a], Y. V. Kalyuzhnyi[b,*], T. Patsahan[b], C. M^{c}Cabe[a]

[a] *Department of Chemical and Biochemical Engineering, Vanderbilt University, Nashville, Tennessee 37235-1604, USA*
[b] *Institute for Condensed Matter Physics NASU, Lviv, Ukraine*

Abstract

A simple analytical theory for the thermodynamic properties of a multicomponent liquid mixture adsorbed in a random porous media is proposed. The mixture is modeled by an n-component fluid of hard-sphere Morse (HSM) particles and the media is represented by the matrix of HSM obstacles randomly distributed in a configuration of HS fluid quenched at equilibrium. We combine scaled particle theory (SPT) and the corresponding version of the second-order Barker-Henderson (BH2) perturbation theory to describe the thermodynamics of the system. To assess the accuracy of the theory, Monte Carlo computer simulations are performed to determine the structure of the corresponding reference system and the chemical potential of the HSM liquid confined in a random HSM matrix. Based on agreement between the theoretical predictions and Monte Carlo simulation data, the structure of the reference system is shown to be accurately predicted using radial distribution functions of the $n+1$-component hard-sphere mixture with the n component representing the fluid and the one component representing the matrix obstacles. Theoretical predictions for the chemical potential are also in a very good agreement for the model for systems with weak fluid-matrix attractive interactions, though slight deviations are ob-

*Corresponding author

served as the strength of the fluid-matrix attraction and/or matrix density is increased. With minimal adjustment of the HSM potential, the phase behavior of the Lennard-Jones and square-well fluids adsorbed in the matrix are also described. Due to its simplicity, the theory could be used in a number of applications to predict the properties of simple fluid mixtures with any number of components adsorbed in the porous media.

Keywords:
adsorption, separations, theory, computer simulation, hard-sphere,
Lennard-Jones, square-well, equation of state

---

1. Introduction

Understanding the thermodynamic properties and phase behavior of fluids and fluid mixtures adsorbed in porous media is of substantial interest for both fundamental science and engineering applications [1, 2, 3, 4]. Porous materials are widely used as adsorbents in numerous technological processes, such as filtration and purification, heterogeneous catalysis, adsorption and separations. The properties of the fluids confined in porous media are known to be markedly different from those in the bulk, which represents a challenge for their understanding and description on the molecular level. For example, the liquid-gas phase diagrams of ^{4}He[5], N_2 [6], and the mixture of isobutyric acid and water [7] confined in dilute silica gel are much narrower than those in the bulk, with the critical points shifted toward the lower temperatures.

Describing the thermodynamics and phase behavior of fluids in porous media is challenging due to the necessity of taking into account the effects of confinement, the fluid-media interaction, the random nature of the pores and their interconnection, etc. Additionally, the phase behavior of adsorbed fluids is very sensitive to the microscopic structure of the adsorbent. Even for porous materials with the same geometrical and statistical properties, such as porosity, size of the obstacles, and distribution of pore sizes, the corresponding fluid phase diagrams can be qualitatively quite different, e.g. having either one or two critical

points [8]. However, since the pioneering work of Madden and Glandt [9], Madden [10] and subsequent important work of Given and Stell [11], considerable progress has been achieved in the theoretical description of the structural properties and thermodynamics of fluids confined in porous media. In [9, 10, 11], the porous medium is modeled as a quenched disordered configuration of particles. The properties of the liquids adsorbed in such medium (the so-called matrix) are described using the corresponding version of the Ornstein-Zernike (OZ) equation called the replica OZ (ROZ) equation, supplemented by analogues of the standard closures of the OZ equation utilized in liquid state theory. In the meantime a number of extensions and modifications of the ROZ approach have been developed and applied (see [4, 12] and references therein). These include extensions of the ROZ theory in the framework of the reference interaction site model (RISM) approach [13, 14, 15] and multi-density integral equation formalism of Wertheim for associating fluids [16, 17, 18, 19, 20, 21], extensions of the ROZ equation's treatment of systems with Coulombic interactions [22, 23] and inhomogeneous systems [24, 25]. In addition to the ROZ approach density functional theory based approaches for inhomogeneous systems have also been proposed [26, 27, 28].

Similar to the regular OZ approach, straightforward application of the ROZ theory is difficult as there are a substantial region of thermodynamic states for which no convergent solutions to the ROZ equation can be found. In addition, none of the closures of the ROZ equation proposed are amenable to an analytical solution. Therefore, most of the theoretical studies of the phase behavior of liquids confined in porous media are based on the application of different approximate perturbation schemes with ROZ equations used to calculate the thermodynamic and/or structural properties of the corresponding reference system [29, 30, 31, 32, 33, 34, 35, 36]. In the papers of Kierlik et al. [30, 31, 35], Trokhymchuk et al. [34] and Patsahan et al. [36] the contribution of the attractive part of the interaction was calculated using the numerical solution of the ROZ with a mean spherical approximation (MSA) type of the closure.

Recently, scaled particle theory (SPT) was extended and applied to predict

the properties of the hard-sphere fluid in porous media [37, 38, 39, 40]. The media was represented by a matrix of hard-sphere obstacle particles randomly placed in a configuration of HS fluid quenched at equilibrium. Unlike ROZ theory, this proposed version of SPT provides a closed form analytical expressions for the thermodynamics of the system. This feature of SPT is very useful, since it enables one to use an analytical description of the reference system in various thermodynamic perturbation theories. Furthermore, predictions from the present version of SPT are perhaps the most accurate in comparison with predictions of the currently available theoretical methods for hard-sphere systems, i.e. ROZ theory.

Additionally, the phase behavior of several model liquids adsorbed in porous media have been studied using the SPT description of the corresponding reference systems. These studies include applications of the Barker-Henderson (BH) perturbation theory to the Lennard-Jones (LJ) fluid [41], the high temperature approximation to the polydisperse hard-sphere Yukawa fluid [42], Wertheim's thermodynamic perturbation theory (TPT) to hard-sphere network forming [43] and polydisperse square-well (SW) chain [44] fluids, the associative mean spherical approximation (AMSA) [45] and the collective variable method [46] to a charged hard-sphere fluid.

Confined fluid properties have also been actively studied using simulation methods, with an emphasis on Monte Carlo (MC) methods. The majority of these simulations focus on describing the LJ fluid under confinement conditions through various MC methods, such as standard MC [47], grand-canonical MC [48, 49, 50, 51], and Gibbs ensemble MC [52, 8]. Confined SW fluids have also been studied using grand-canonical transition-matrix MC [53]. However, while LJ and SW fluids are well represented, both simulation and theoretical approaches that utilize other potentials for the model fluid have been widely neglected. We note that computer simulations of the phase behavior of fluids adsorbed in porous media are challenging. During each simulation, the fluid properties have to be averaged with respect to the different realizations of the matrix (i.e., porous media), which is time consuming, since each realization re-

quires a separate simulation. Also it is generally not clear how many realizations are needed and what size of the matrix sample should be used in order to obtain sufficiently accurate predictions.

In this paper, we propose a simple analytical theory for predicting the thermodynamic properties and phase behavior of liquid mixtures with any number of components confined in random porous media. The theory is based on the combination of SPT and second-order BH (BH2) perturbation theory. The liquid is represented by an n-component mixture of the hard-sphere Morse (HSM) model and the porous media is modeled by the HS fluid quenched at equilibrium. The choice of the HSM model and SPT description of the reference system enables us to formulate a completely analytical version of the second-order BH perturbation theory for systems with an arbitrary number of components. Note that previous studies of the phase behavior are based on the numerical solutions of the ROZ equation, which is rather combersome to use even in the one-component case and quickly becomes impractical as the number of components increases. The accuracy of the theory, as well as its applicability, is demonstrated by comparison of the theoretical predictions against corresponding MC simulations.

2. Model

We consider a simple liquid mixture confined in a random porous medium. The liquid is modeled by a multicomponent mixture of hard spheres of different size with an additional attractive Morse potential. For the porous medium the model suggested by Madden and Glandt [9, 10] is used, in which a matrix of hard-sphere obstacles formed by a fluid of hard particles quenched at equilibrium is used. In addition to the hard-sphere interaction, the particles of the liquid interact with the matrix obstacles via the attractive Morse potential. The pair potential acting between the particles of the system is

$$U_{ij}(r) = U_{ij}^{(hs)}(r) + U_{ij}^{(M)}(12), \tag{1}$$

where i, j denotes the particle species and takes the values $0, \ldots, n$, $U_{ij}(r)^{(hs)}$ is the hard sphere potential

$$U_{ij}^{(hs)}(r) = \begin{cases} \infty, & \text{for } r < \sigma_{ij} \\ 0, & \text{for } r > \sigma_{ij} = (\sigma_i + \sigma_j)/2 \end{cases}, \tag{2}$$

σ_i is the hard-sphere diameter of the particle of species i, and $U_{ij}(r)^{(M)}$ is the Morse potential

$$U_{ij}^{(M)}(r) = \begin{cases} 0, & \text{for } r < \sigma_{ij} \\ -\epsilon_{ij}^{(M)} \exp\left[-z_{ij}(r - \sigma_{ij})\right], & \text{for } r > \sigma_{ij} \end{cases} \tag{3}$$

Here, as usual, $i = 0$ denotes hard-sphere obstacles of the matrix, $\epsilon_{00}^{(M)} = 0$ and the screening parameter z_{ij} was chosen to be $z_{ij} = 1.8/\sigma_1$.

3. Theory

Theoretical description of the model at hand is carried out using BH2 perturbation theory in combination with scaled particle theory [42, 44, 54]. We assume that the Helmholtz free energy of our liquid mixture can be written as follows:

$$A = A_{ref} + \Delta A_1^{(M)} + \Delta A_2^{(M)}, \tag{4}$$

where A_{ref} is Helmholtz free energy of the reference system, and A_1 and A_2 the first and second perturbation terms respectively,

$$\frac{\beta \Delta A_1^{(M)}}{V} = 2\pi\beta \sum_{ij} \rho_i \rho_j \int_0^\infty dr\, r^2 U_{ij}^{(M)}(r) g_{ij}^{(ref)}(r) =$$

$$= 2\pi\beta \sum_{ij} \epsilon_{ij}^{(M)} \rho_i \rho_j e^{z_{ij}\sigma_{ij}} \frac{\partial G_{ij}^{(ref)}(s)}{\partial s}|_{s=z_{ij}}. \tag{5}$$

and

$$\frac{\beta \Delta A_2^{(M)}}{V} = -\pi\beta^2 K^{(ref)} \sum_{ij} \rho_i \rho_j \int_0^\infty dr\, r^2 [U_{ij}^{(M)}(r)]^2 g_{ij}^{(ref)}(r) =$$

$$= \pi\beta^2 K^{(ref)} \sum_{ij} \left(\epsilon_{ij}^{(M)}\right)^2 \rho_i \rho_j e^{2z_{ij}\sigma_{ij}} \frac{\partial G_{ij}^{(ref)}(s)}{\partial s}|_{s=2z_{ij}}. \tag{6}$$

Here $g_{ij}^{(ref)}(r)$ is the radial distribution function (RDF) of the reference system, $G_{ij}^{(ref)}(s)$ is the Laplace transform of $g_{ij}^{(ref)}(r)$,

$$G_{ij}^{(ref)}(s) = \int_0^\infty dr\ re^{-sr} g_{ij}^{(ref)}(r), \tag{7}$$

$K^{(ref)}$ is isothermal compressibility of the reference system, i.e

$$K^{(ref)} = \left(\frac{\partial \rho}{\partial(\beta P_{ref}))} \right), \tag{8}$$

P_{ref} is the pressure of the reference system, $\beta = 1/k_B T$, T is the temperature, ρ_i is the number density of the component i and $\rho = \sum_{i=1}^{n} \rho_i$.

The reference system is represented by the multicomponent hard-sphere fluid confined in the random porous medium. The thermodynamic properties of the system are calculated using a recently proposed version of scaled particle theory (SPT) [39]. In the framework of SPT, explicit analytical expressions for the Helmholtz free energy and chemical potential of the n-component hard-sphere fluid confined in the hard- sphere random matrix have been derived [37, 39, 38, 40]. To avoid repetition, we do not present them here and refer the reader to the original publications.[37, 39, 38, 40]. However, for the sake of completeness, the SPT expressions for the Helmholtz free energy, chemical potential and compressibility of the one-component hard-sphere fluid in the matrix, which will be used in our numerical calculations are provided below. We have

$$\frac{\beta A_{hs}}{N} = \beta\mu_{hs} - \frac{\beta P_{hs}}{\rho}, \tag{9}$$

where

$$\frac{\beta P_{hs}}{\rho} = \frac{1}{1-\eta/\phi_0}\frac{\phi_0}{\phi} + \left(\frac{\phi_0}{\phi} - 1\right)\frac{\phi_0}{\eta}\ln\left(1 - \frac{\eta}{\phi_0}\right) + \frac{a}{2}\frac{\eta/\phi_0}{(1-\eta/\phi_0)^2} + \frac{2b}{3}\frac{(\eta/\phi_0)^2}{(1-\eta/\phi_0)^3}, \tag{10}$$

$$\beta\mu_{hs} = \ln\left(\Lambda_1^3\rho\right) + \beta\mu_1^{(ex)} - \ln\left(1 - \frac{\eta}{\phi_0}\right) + \frac{\eta(\phi_0 - \phi)}{\phi_0\phi(1-\eta/\phi_0)} + (1+a)\frac{\eta/\phi_0}{(1-\eta/\phi_0)} + \frac{(a+2b)}{2}\frac{(\eta/\phi_0)^2}{(1-\eta/\phi_0)^2} + \frac{2b}{3}\frac{(\eta/\phi_0)^3}{(1-\eta/\phi_0)^3}, \tag{11}$$

$$K_{hs} = \left[\frac{1}{1-\eta/\phi_0} + \frac{\eta/\phi}{(1-\eta/\phi_0)^2} + a\frac{\eta/\phi_0}{(1-\eta/\phi_0)^3} + 2b\frac{(\eta/\phi_0)^2}{(1-\eta/\phi_0)^4}\right]^{-1}, \tag{12}$$

and $\eta_0 = \pi\rho_0\sigma_0^3/6$, $\phi_0 = 1-\eta_0$, $\eta = \pi\rho_1\sigma_1^3/6$ and $\phi = \exp\left(-\beta\mu_1^{(ex)}\right)$. Here

$$a = 6 + \frac{3\eta_0\tau\left(\tau+4\right)}{1-\eta_0} + \frac{9\eta_0^2\tau^2}{(1-\eta_0)^2}, \qquad b = \frac{9}{2}\left(1+\frac{\tau\eta_0}{1-\eta_0}\right)^2, \tag{13}$$

$$\begin{aligned}\beta\mu_1^{(ex)} = &-\ln\left(1-\eta_0\right) + \frac{9\eta_0^2}{2(1-\eta_0)^2} - \eta_0 Z_0 + \left[3\eta_0 Z_0 - \frac{3\eta_0(2+\eta_0)}{(1-\eta_0)^2}\right](1+\tau) \\ &- \left[3\eta_0 Z_0 - \frac{3\eta_0(2+\eta_0)}{2(1-\eta_0)^2}\right](1+\tau)^2 + \eta_0 Z_0(1+\tau)^3,\end{aligned} \tag{14}$$

and $Z_0 = (1+\eta_0+\eta_0^2)/(1-\eta_0)^3$ and $\tau = \sigma_1/\sigma_0$.

The structural properties of the reference system are calculated assuming that the RDFs $g_{ij}^{(ref)}(r)$ can be approximated by the RDFs of the $n+1$-component hard-sphere mixture $g_{ij}^{(hs)}(r)$ with n components representing the reference system and one component representing the matrix of the hard-sphere obstacles. To validate this assumption computer simulations have been performed and the results obtained compared against the corresponding theoretical results. Theoretical pair distribution functions have been calculated using the Percus-Yevick (PY) approximation. One substantial advantage of the PY approximation is that the closed form analytical expression for the Laplace transforms of the hard-sphere RDFs $G_{ij}^{(hs)}(s)$, which enter in to the expressions for the Helmholtz free energy (5) and (6), are available [55].

The chemical potential, μ_i, and pressure, P, of the system are calculated using standard thermodynamical relations, i.e.

$$\mu_i = \mu_i^{(ref)} + \Delta\mu_i, \qquad P = P_{ref} + \Delta P, \tag{15}$$

where

$$\Delta\mu_i = \frac{\partial}{\partial\rho_i}_{|\left\{\rho_{j\neq i}\right\}}\left(\frac{\Delta A_1}{V} + \frac{\Delta A_2}{V}\right), \tag{16}$$

$$\Delta P = \sum_{i=1}^{n}\rho_i\Delta\mu_i - \frac{\Delta A_1}{V} - \frac{\Delta A_2}{V}. \tag{17}$$

4. MC simulations details

To assess the accuracy of the theoretical approach proposed, Monte-Carlo (MC) computer simulations[56] have been performed of the same model as that studied theoretically, thus providing exact model properties and the ability to directly test the theory. The simulated system consists of fluid particles immersed in the environment of a matrix formed by a frozen configuration of randomly dispersed impenetrable hard spheres (HS matrix). We consider the system in a simulation box of a cubic shape with periodic boundary conditions applied along three dimensions. The number of the matrix particles N_0 is varied depending on the packing fraction η_0 of the system and the HS particle diameter $\sigma_0 = \sigma_1/\tau$, where: $\eta_0 = \pi\sigma_0^3 N_0/L^3/6$.

Canonical (NVT) MC simulations [56] were performed to determine the RDFs of the reference system. The fluid-fluid $g_{11}^{(ref)}(r)$ and fluid-matrix $g_{01}^{(ref)}(r)$ RDFs were obtained from NVT simulations of a hard-sphere fluid confined in a disordered hard-sphere matrix at various packing fractions of fluid, η_1, and matrix, η_0, particles. Several different values for the size ratio of fluid and matrix particles τ have been considered. The number of the matrix particles in the system N_0 are chosen depending on their size, i.e., N_0 = 10000, 6000, 4000 and 2000, for τ = 1, 1/2, 1/3 and 1/5, respectively. For each set of system parameters, eight random matrix configurations are studied and the RDFs are averaged over these matrix realizations. Each simulation run consists of $5 \cdot 10^5$ simulation steps for system equilibration and additional 10^5 steps for production. At each step, N_1 trial moves of particles are performed, where N_1 is the number of fluid particles. The maximum displacement for trial moves of fluid particles was adjusted to reach the acceptance rate around 75%. The RDFs were calculated by sampling the configuration every 5 steps. To speed up simulations the linked-cell algorithm with a cell size equal to $2\sigma_1$ was applied [56].

Grand-canonical MC (GCMC) simulations were performed to obtain the average density of a HSM fluid confined in a disordered hard-sphere matrix

at a fixed chemical potential and constant temperature. [56]. The system was simulated in a box of the size $L = 20\sigma_{11}$ and a cut-off distance of $r_c = 10\sigma_1$ used for both the fluid-fluid and fluid-matrix interactions. The number of matrix particles N_0 was adjusted according to the chosen combination of η_0 and τ. Two values of the matrix packing fraction, $\eta_0 = 0.1$ and 0.15, have been studied and are typical values for a wide range of mesoporous materials [2, 3, 4]. The screening parameter z_{ij} of the HSM potential (3) is $z_{ij} = 1.8/\sigma_1$, indicating that the value of the cut-off distance used is sufficiently large.

All GCMC simulations are performed at the temperature $k_BT/\epsilon_{11}^{(M)} = 2$, which is very close to the critical temperature of the bulk fluid, but still belongs to the supercritical region. For each set of parameters the system is fully equilibrated starting from a random initial configuration with fluid particles of density $\rho^* = 0.1$. Each simulation step consists of translational trial moves with the maximum displacement $0.2\sigma_{11}$ and insertion/removal attempts. The ratios of translation and insertion/removal trials are set to 80% and 20%, respectively. The total number of trials during one simulation step is chosen equal to the number of fluid particles N_1. The number of steps needed to equilibrate the systems at the considered chemical potentials is typically found to be less than 10^5. Afterwards, the fluid density is averaged during at least 10^5 simulation steps. To improve statistics at substantially low fluid densities ($\rho_1\sigma_{11}^3 < 0.01$), the number of simulation steps is increased to 10^6. In general, the relative error of the densities obtained at the different values of the chemical potential was around 1% or better. For the sake of comparison a HSM fluid in the bulk is also simulated. Finally, we note that while computer simulations of fluids adsorbed in porous media are challenging as discussed above, the simulations performed herein are carried out at temperatures above the critical temperature and therefore they are expected to be sufficiently accurate.

5. Results and discussion

5.1. Structure of the reference system

We present theoretical predictions for the RDFs of the reference system $g_{11}^{(ref)}(r)$ and $g_{01}^{(ref)}(r)$ in figures 1-4 compared against the corresponding computer simulation predictions. Four versions of the model matrix with different porosity ($\phi_0 = 1 - \eta_0$) and different ratios of the sizes of the obstacle and fluid particles τ ($\eta_0 = 0.1058$ and $\tau = 1$ (figure 1), $\eta_0 = 0.2206$ and $\tau = 1/2$ (figure 2), $\eta_0 = 0.2972$ and $\tau = 1/3$ (figure 3), $\eta_0 = 0.3901$ and $\tau = 1/5$ (figure 4)) are considered. For each set of η_0 and τ we present results for the RDFs at high and low values of the fluid packing fraction η. In all cases studied, very good quantitative agreement between the theoretical and computer simulation results can be observed for almost all values of the distance between the particles r. Slightly less accurate predictions from the theory can be seen only in close vicinity to the contact distance for the RDF $g_{11}^{(ref)}(r)$ at higher densities and for the RDF $g_{01}^{(ref)}(r)$ at both, high and low densities.

5.2. Thermodynamics of the hard-sphere Morse liquid confined in the matrix

In figures 5-7 theoretical and computer simulation results for the excess chemical potential as a function of the density of the HSM liquid confined in the matrix are presented. We have studied three different sets of the model parameters for the matrix, i.e. $\eta_0 = 0.1$ and $\tau = 1$ (figure 5), $\eta_0 = 0.15$ and $\tau = 1$ (figure 6), $\eta_0 = 0.1$ and $\tau = 3/2$ (figure 7). For each version of the matrix model parameters three values of the interaction energy $\epsilon_{01}^{(M)}$ ($\epsilon_{01}^{(M)}/\epsilon_{11}^{(M)} = 0, 1, 1.5$) are considered. The temperature of the system is $T^* = k_B T/\epsilon_{11}^{(M)} = 2$.

In general, the agreement between the theoretical predictions and simulations is good. For the model with $\epsilon_{01} = 0$, the theoretical predictions are very accurate. As the strength of matrix-fluid attraction ϵ_{01} is increased, the theory provides slightly less accurate results for small values of ρ^* and larger values of η_0. This decrease in the accuracy of the theoretical results is due to relatively less accurate predictions of the theory for $g_{01}(r)$, since at these values of ρ^*

and η_0 the contribution to the Helmholtz free energy (5) and (6) due to the matrix-fluid correlations become larger.

5.3. Liquid-vapor phase behavior

Results for the phase behavior of the model are given in figures 8 and 9. In figure 8 the liquid-vapor phase diagram of the HSM fluid confined in the hard-sphere matrix at three different values of the matrix packing fraction $\eta_0 = 0, 0.1, 0.2$ and two different values of the matrix-fluid size ratio $\tau = 1, 1/2$ are presented. As one would expect with the increase of the matrix packing fraction the phase envelope and critical point shifts in the direction of lower temperatures and lower densities. This effect is more pronounced for the models with larger value of τ. The effects of the attraction between fluid particles and obstacles of the matrix are shown in figure 9. Here we consider the model with $\eta_0 = 0.1$, $\tau = 1$ and $\epsilon_{01}^{(M)} = 0$, $\epsilon_{01}^{(M)}/\epsilon_{11}^{(M)} = 1$, $\epsilon_{01}^{(M)}/\epsilon_{11}^{(M)} = 3$ and $\epsilon_{01}^{(M)}/\epsilon_{11}^{(M)} = 6$. With the increase of the strength of fluid-matrix interaction, $\epsilon_{01}^{(M)}/\epsilon_{11}^{(M)}$, from 0 to 1 the critical temperature and density increase. With further increase of the strength of the attraction up to $\epsilon_{01}^{(M)}/\epsilon_{11}^{(M)} = 6$ the critical temperature noticeably decreases and the critical density becomes almost twice as large. This behavior can be attributed to the competition between fluid-fluid and fluid-matrix interactions. With the increase of the fluid-matrix attraction the formation of the liquid phase requires lower temperatures and higher densities.

Finally in figures 10-14 we compare our theoretical predictions for the liquid-gas phase diagram for the LJ and hard-sphere SW fluids confined in the LJ and hard-sphere matrices against the corresponding computer simulation predictions from the literature [8, 53], as computer simulation results for the phase behavior of the HSM model are not available. We note that these computer simulations were carried out taking into account only one matrix realization. In [8], the authors use a truncated LJ potential

$$U_{11}^{(LJ)}(r) = \begin{cases} 4\epsilon_{11}^{(LJ)} \left[\left(\frac{\sigma_{11}^{(LJ)}}{r} \right)^{12} - \left(\frac{\sigma_{11}^{(LJ)}}{r} \right)^{6} \right] & \text{for } r < r_c \\ 0, & \text{for } r > r_c \end{cases} . \qquad (18)$$

for the interaction between the liquid particles and either the hard-sphere potential or LJ potential analogous to (18) for the interaction between fluid and matrix particles. Description of the LJ model is carried out using the BH prescription [57] for the effective hard-sphere sizes σ_{11} and σ_{01}. For the HSM potential energy parameter $\epsilon_{11}^{(M)}$ we have used the value obtained as a result of fitting of the corresponding computer simulation bulk phase diagrams and for $\epsilon_{01}^{(M)}$ we have: $\epsilon_{01}^{(M)} = \epsilon_{11}^{(M)}(\epsilon_{01}^{(LJ)}/\epsilon_{11}^{(LJ)})$. Description of the model with hard-sphere SW interaction potential, i.e.

$$U_{11}^{(SW)}(r) = \begin{cases} \infty, & \text{for } r < \sigma_{11} \\ -\epsilon_{11}^{(SW)}, & \text{for } \sigma_{11} \le r < \lambda\sigma_{11} \\ 0, & \text{for } \lambda\sigma_{11} \le r \end{cases} , \tag{19}$$

is carried out following the scheme similar to that used above. Explicit expressions for the temperature dependence of $\epsilon_{11}^{(M)}$ in the case of LJ fluid and SW fluid are presented in the Appendix. In both cases the value of the HSM potential decay parameter was chosen to be $z = 1.8/\sigma_{11}^{(LJ)}$.

In general, the agreement between the theoretical predictions and simulation data is good. The theory correctly reproduces the effects of the confinement due to changes in both the size ratio of the fluid and matrix particles (figure 10) and in the packing fraction of the matrix η_0 (figures 11 and 14). With the increase of the matrix particles size at constant η_0 the average size of the pores increases, which makes the effects of confinement weaker. As a result the critical temperature and density of the fluid adsorbed in the matrix with larger obstacles is larger than those of the fluid in the matrix with smaller obstacles (figure 10). On the other hand, increasing the matrix packing fraction η_0 decreases the porosity and increases the effects of confinement. This effect can be seen in figures 11 and 14, where due to the increase of η_0 the phase envelope shifts in the direction of lower temperatures and densities. Here theoretical predictions are in relatively good agreement with computer simulation predictions for lower and intermediate values of η_0, i.e. $\eta_0 = 0.05$ and $\eta_0 = 0.1$. In particular, for the SW fluid, the accuracy of our theory is similar to that of Hvozd et al. [44]

(figure 14). In the latter study, the authors apply the BH2 approach directly to the SW model in question.

For $\eta_0 = 0.1$ computer simulation for the LJ fluid in the matrix [8] shows the existence of the two phase transitions with two critical points: one located at lower density and higher temperature and the other at higher density and lower temperature. At the same time, MC computer simulations, carried out for the SW fluid in the matrix [53] with the same value of η_0, shows the appearance of a single phase transition. In both cases, the theory predicts the existence of only one phase transition. However, we note that the phase behavior of the fluid adsorbed in the porous media is very sensitive to even subtle differences in the matrix structure and for two different realizations of the matrix with the same porosity, size of the obstacles and distribution of the pore sizes, computer simulations can produce the phase diagram with and without two phase transitions [8] . Therefore, the existence of the two phase transitions for the LJ model at hand is still questionable [50, 58]. With further decrease of the matrix porosity up to $\eta_0 = 0.2$, the theoretical phase envelope shifts towards the lover temperatures and densities (figure 11). In contrast, the computer simulation phase diagram shifts in the direction of slightly higher temperatures and lower densities and becomes substantially more narrow. We believe that this disagreement can be explained by the sensitivity of the phase behavior to the matrix structure, generated in the computer simulations. Next in figures 12 and 13, we compare predictions of the theoretical predictions and simulation results for the effects of attraction between LJ fluid and matrix particles. We consider the case of equal (figure 12) and different (figure 13) sizes of the fluid and matrix particles. In both cases, an increase in the fluid-matrix attraction leads to a shift of the phase diagram to higher temperatures. At the same time, while the theoretical phase diagram shifts to higher densities, the computer simulation phase diagram for $\epsilon_{01}^{LJ)}/\epsilon_{11}^{(LJ)} = 1$ is shifted in the opposite direction to lower densities (figure 12) and for $\epsilon_{01}^{LJ)}/\epsilon_{11}^{(LJ)} = 1.25$ it is moved towards the higher densities (figure 13). In our opinion this nonmonotonic behavior can be also attributed to the difficulties in performing computer simulations of the systems in question,

in particular due to insufficient number of matrix realizations accounted.

6. Conclusions

In this paper we propose a simple analytical theory for thermodynamics of the multicomponent simple liquid mixtures confined in the porous media. The media is represented by the matrix of hard-sphere obstacles randomly placed in a configuration of a HS fluid quenched at equilibrium. A simple fluid mixture is modeled by the n-component hard-sphere mixture with additional attractive Morse potential between liquid particles and between the particles of the matrix and liquid particles. For the theoretical description, we combine SPT and second-order BH perturbation theory, appropriately modified to account for the absence of the interaction between the matrix particles. SPT is used to describe the thermodynamics of the reference system. We have shown that the structure of the reference system can be accurately predicted using PY RDFs of the $n+1$-component hard-sphere mixture with the n component representing the fluid and one component representing the matrix obstacles. Agreement between theoretical and computer simulation predictions is very good for fluid-fluid RDFs and slightly less accurate for fluid-matrix RDFs at all densities and size ratios studied. It is also demonstrated that BH2 perturbation theory for the $n+1$-component HSM liquid can be used to give sufficiently accurate predictions for the thermodynamics of the n-component fluid confined in the matrix with HSM obstacles. Theoretical predictions for the chemical potential are in a very good agreement for the model with weak fluid-matrix attraction and becomes less accurate with the increase of the fluid-matrix attraction and matrix density. Our SPT-BH2 approach is able to correctly predict the effects due to the changes in the matrix density, fluid-matrix particles size ratio and strength of the of fluid-matrix interaction of the liquid-gas phase behavior. With a minimal adjustment of our HSM potential we were able to reproduce with a reasonable accuracy computer simulation results for the phase behavior of the LJ and hard-sphere SW fluids confined in the porous media. Due to its simplicity, the theory

can be used to study the properties of a simple fluid mixture with any number of components adsorbed in the hard-sphere matrix. Taking into account the isomorphism of the fluid adsorbed in disordered hard-sphere matrix [39] we expect that our theory can be applied also to describe the properties of the fluids confined in the matrices with the other hard-core morphologies.

7. Acknowledgment

A.K.N and C.MC gratefully acknowledge financial support from the National Science Foundation under grant number CBET-1805126. Y.V.K. and T.P. also acknowledge support from the Ministry of Education and Science of Ukraine (grant No. M/116-2019).

References

[1] T.J. Barton, L.M. Bull, W.G. Klemperer, D.A. Loy, B. McEnaney, M. Misono, P.A. Monson, G. Pez, G.W. Scherer, J.C. Vartuli, O.M. Yaghi, Chem. Mater. 11 (1999) 2633.

[2] L.D. Gelb, K.E. Gubbins, R. Radhakrishnan, M. Sliwinska-Bartkowiak, Rep. Prog. Phys. 62 (1999) 1573.

[3] G.Q. Lu, X.S. Zhao, Nanoporous Materials: Science and Engineering (Series of Chemical Engineering vol 4) London: Imperial College Press, (2004).

[4] O. Pizio, In Computational Methods in Surface and Colloid Science; Borowko, M., Ed.; CRC Press, 2019; pp 293.

[5] A.P.Y. Wong, M.H.W. Chan, Rev. Lett. 65 (1990) 2567.

[6] A.P.Y. Wong, S.B. Kim, W.I. Goldburg, M.H.W. Chan, Phys. Rev. Lett. 70 (1993) 954.

[7] Z. Zhuang, A.G. Casielles, D.S. Cannell, Phys. Rev. Lett. 77 (1996) 2969.

[8] J.K. Brennan, W. Dong, J. Chem. Phys. 116 (2002) 8948.

[9] W.G. Madden, E.D. Glandt, J. Stat. Phys. 51 (1988) 537.

[10] W.G. Madden, J. Chem. Phys. 96 (1992) 5422.

[11] J.A. Given, G. Stell, J. Chem. Phys. 97 (1992) 4573.

[12] L. Sarkisov, P.R. Van Tassel, J. Phys.: Condens. Matter 20 (2008) 1.

[13] A. Kovalenko, F. Hirata, J.Chem.Phys. 115 (2001) 8620.

[14] D. Chandler, J.Phys.:Condens.Matter 3 (1991) F1.

[15] A.P. Thompson, E.D. Glandt, J. Chem. Phys. 99 (1993) 8325.

[16] A. Trokhymchuk, O. Pizio, M. Holovko, S. Sokolowski, J. Chem. Phys. 106 (1997) 200.

[17] G.A. Orozco, O. Pizio, S. Sokolowski, A. Trokhymchuk, Mol. Phys. 91 (1997) 625.

[18] O. Pizio, Y. Duda, A. Trokhymchuk, S. Sokolowski, J. Mol. Liq. 76 (1998) 183.

[19] P. Padilla, O. Pizio, A. Trokhymchuk, C. Vega, J. Phys. Chem. B 102 (1998) 3012.

[20] B.M. Malo, O. Pizio, A. Trokhymchuk, Y. Duda, J. Coll. Interf. Sci. 211 (1999) 387.

[21] T. Urbic, V. Vlachy, O. Pizio, K.A. Dill, J. Mol. Liq. 112 (2004) 71.

[22] V. Vlachy, B. Hribar, O. Pizio, Phys. A: Stat. Mech. 314 (2002) 156.

[23] V. Vlachy, H. Dominguez, O. Pizio, J. Phys. Chem. B 108 (2004) 1046.

[24] O. Pizio, S. Sokolowski, Phys. Rev. E 56 (1997) R63.

[25] A. Kovalenko, S. Sokołowski, D. Henderson, O. Pizio, Phys. Rev. E 57 (1998) 1824.

[26] E. Kierlik, P.A. Monson, M.L. Rosinberg, L. Sarkisov, G. Tarjus, Phys. Rev. Lett. 87 (2001) 055701.

[27] J. Landers, G.Y. Gor, A.V. Neimark, Coll. Surf. A 437 (2013) 3.

[28] M. Schmidt, J. Phys.: Condens. Matter 17 (2005) S3481.

[29] D.M. Ford, E. Glandt, Phys. Rev. E 50 (1994) 1280.

[30] E. Kierlik, M.L. Rosinberg, G. Tarjus, P.A. Monson, J. Phys.: Condens. Matter 8 (1996) 9621.

[31] E. Kierlik, M.L. Rosinberg, G. Tarjus, P.A. Monson, J. Chem. Phys. 106 (1997) 264.

[32] A. Kovalenko, O. Pizio, J. Chem. Phys. 108 (1998) 8651.

[33] A. Trokhymchuk, S. Sokolowski, J. Chem. Phys. 109 (1998) 5044.

[34] A. Trokhymchuk, G.A. Orozco, O. Pizio, V. Vlachy, J. Coll. Interf. Sci. 207 (1998) 379.

[35] V. Krakoviack, E. Kierlik, M.L. Rosinberg, G. Tarjus, J. Chem. Phys. 115 (2001) 11289.

[36] T. Patsahan, A. Trokhymchuk, M. Holovko, J. Mol. Liq. 105 (2003) 227.

[37] T. Patsahan. M. Holovko, W. Dong, J. Chem. Phys. 134 (2011) 074503.

[38] W. Dong, X. Chen, Sci. China-Phys. Mech. Astron. 61 (2018) 070501.

[39] M. Holovko, T. Patsahan, W. Dong, Pure Appl. Chem. 85 (2013) 115.

[40] C. Qiao, S. Zhao, H. Liu, W. Dong, Langmuir 35 (2019) 3840.

[41] M.F. Holovko, T.M. Patsahan, V.I. Shmotolokha, Condens. Matter Phys. 18 (2015) 13607.

[42] T.V. Hvozd, Y.V. Kalyuzhnyi, Soft Matter 13 (2017) 1405.

[43] Y.V. Kalyuzhnyi, M. Holovko, T. Patsahan, P.T. Cummings, J. Phys. Chem. Lett. 5 (2014) 4260.

[44] T.V. Hvozd, Y.V. Kalyuzhnyi, P.T. Cummings, J. Phys. Chem. B 122 (2018) 5458.

[45] M. Holovko, T. Patsahan, O. Patsahan, J. Mol. Liq. 228 (2017) 215.

[46] M.F. Holovko, O. Patsahan, T. Patsahan, J. Phys.: Condens. Matter 28 (2016) 414003.

[47] K.S. Page, P.A. Monson, Phys. Rev. E 54 (1996) 6557.

[48] K.S. Page, P.A. Monson, Phys. Rev. E 54 (1996) R29.

[49] M. Alvarez, D. Levesque, J.J. Weis, Phys. Rev. E 60 (1999) 5495.

[50] L. Sarkisov, P.A. Monson, Phys. Rev. E 61 (2000) 7231.

[51] V. De Grandis, P. Gallo, M. Rovere, Phys. Rev. E 70 (2004) 061505.

[52] J.K. Brennan, W. Dong, Phys. Rev. E 67 (2003) 031503.

[53] A.N. Kumar, J.K. Singh, Mol. Phys. 106 (2008) 2277.

[54] T. V. Hvozd, Y. V. Kalyuzhnyi, Condens. Matter Phys. 18 (2015) 13605.

[55] L. Blum, J. S. Hoye, J. Phys. Chem. 81 (1077) 1311.

[56] M.P. Allen, D.J. Tildesley, Computer Simulation of Liquids. 2nd edition, Oxford University Press, Oxford, (2017).

[57] J.A. Barker, D. Henderson, J. Chem. Phys 47 (1967) 4714.

[58] E.V. Vakarin, W. Dong, J.P. Badiali, Physica A 379 (2007) 389.

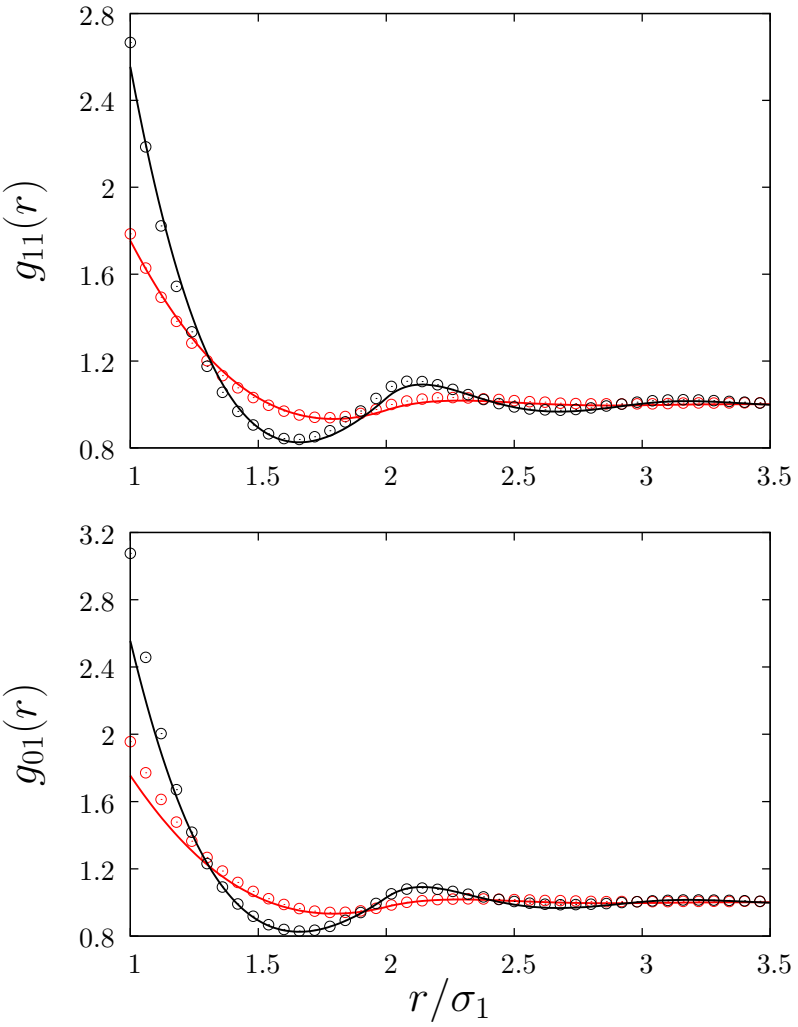

Figure 1: Radial distribution function between fluid hard-sphere particles $g_{11}(r)$ (upper panel) and fluid and matrix hard-sphere particles $g_{01}(r)$ (lower panel) for the hard-sphere fluid confined in a random hard-sphere matrix. Lines represent predictions of the theory and symbols stand for computer simulation results. Here $\tau = 1$, $\eta_0 = 0.1058$, red symbols and lines denote the system with $\eta = 0.1011$ and black symbols and lines denote the system with $\eta = 0.2197$. Here and in figures 2-4 the error in MC simulation predictions do not exceed the size of the symbols in the figure

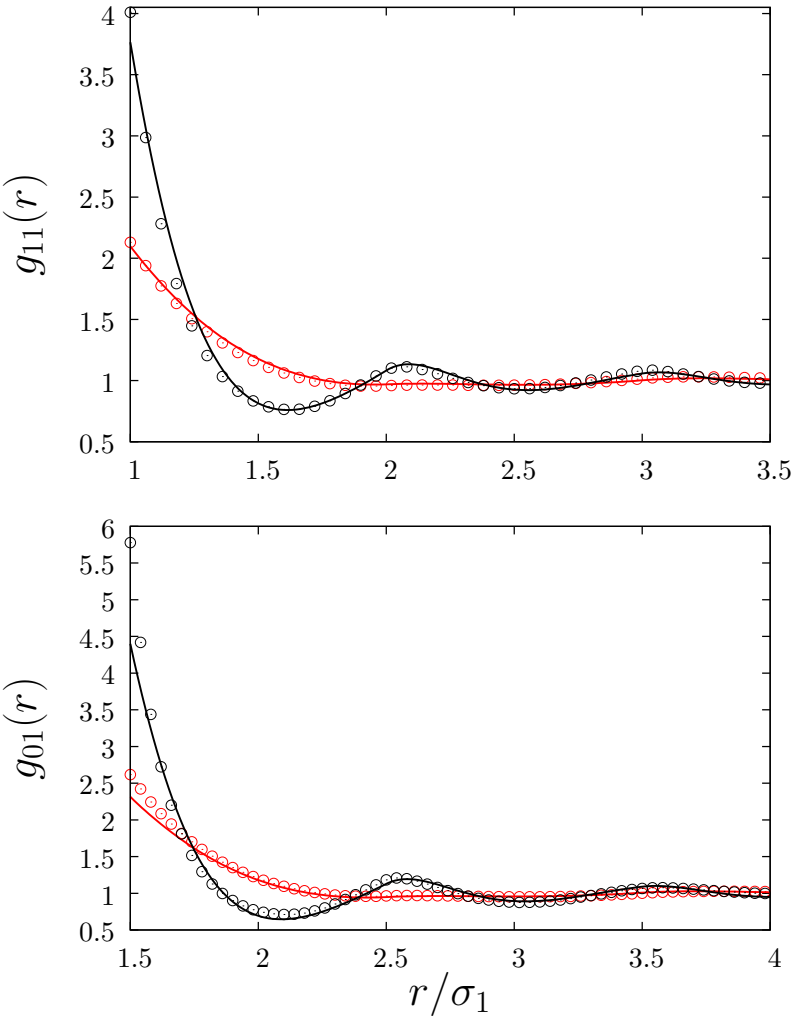

Figure 2: Notation is the same as that in figure 1 except that here $\tau = 1/2$, $\eta_0 = 0.2206$, red symbols and lines denote the system with $\eta = 0.0921$ and black symbols and lines denote the system with $\eta = 0.2469$.

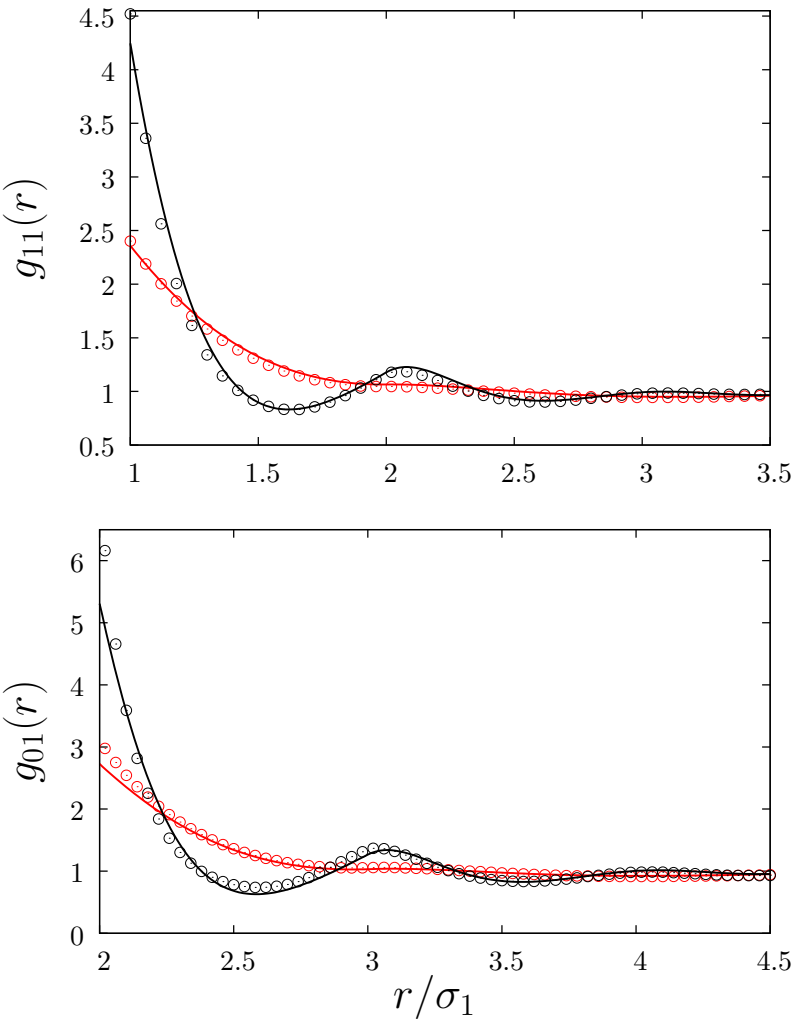

Figure 3: Notation is the same as that in figure 1 except that here $\tau = 1/3$, $\eta_0 = 0.2972$, red symbols and lines denote the system with $\eta = 0.0869$ and black symbols and lines denote the system with $\eta = 0.2263$.

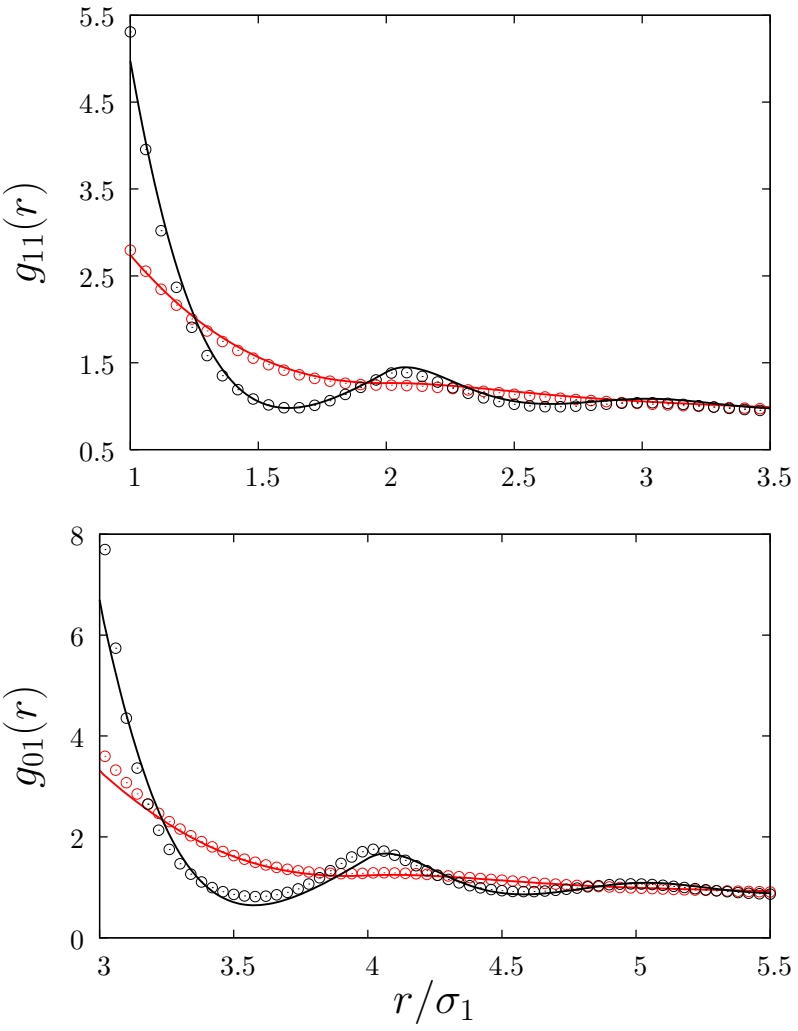

Figure 4: Notation is the same as that in figure 1 except that here $\tau = 1/5$, $\eta_0 = 0.3901$, red symbols and lines denote the system with $\eta = 0.0806$ and black symbols and lines denote the system with $\eta = 0.2020$.

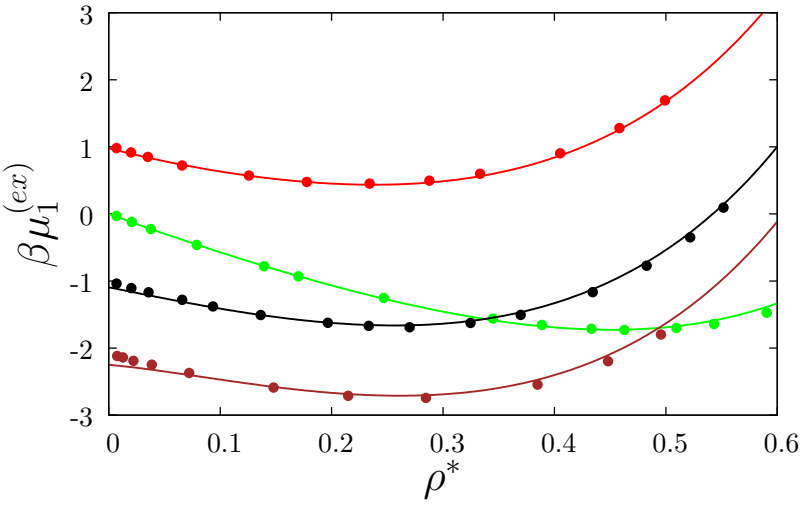

Figure 5: Excess chemical potential $\beta\mu_1^{(ex)}$ of the hard-sphere Morse liquid confined in the matrix at $T^* = 2$ as a function of the liquid density ρ^*. Lines show predictions of the theory and symbols stand for computer simulation results. Here $\tau = 1$, $\eta_0 = 0.1$ and $\epsilon_{01}^{(M)} = 0$ (red lines and symbols), $\epsilon_{01}^{(M)}/\epsilon_{11}^{(M)} = 1$ (black lines and symbols) and $\epsilon_{01}^{(M)}/\epsilon_{11}^{(M)} = 1.5$ (brown lines and symbols). Green line and symbols represent $\beta\mu_1^{(ex)}$ for the hard-sphere Morse liquid in the absence of the matrix and $\rho^* = \rho_1\sigma_1^3$. Here and in figures 6 and 7 the error in MC simulation predictions do not exceed the size of the symbols in the figure

.

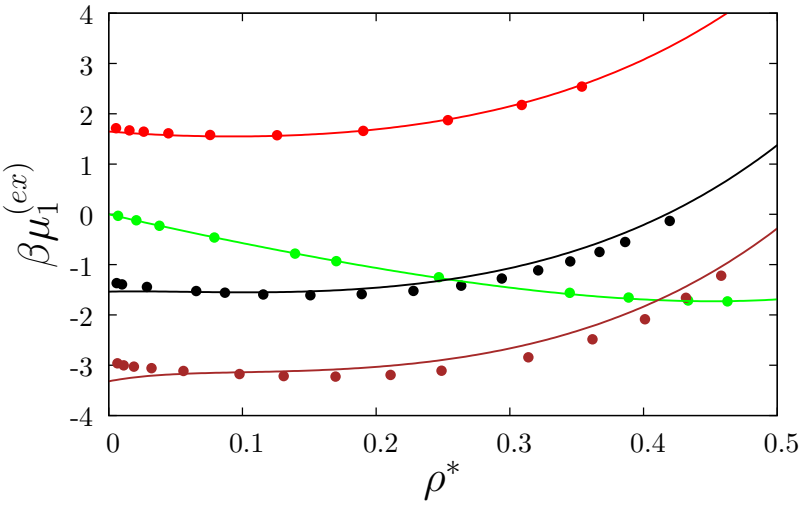

Figure 6: The same as in figure 5 except $\eta_0 = 1.5$.

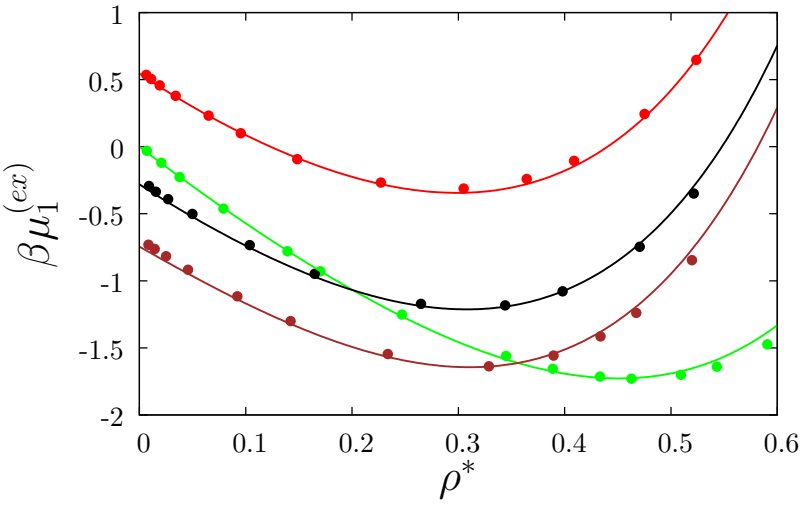

Figure 7: The same as in figure 5 except $\tau = 2/3$.

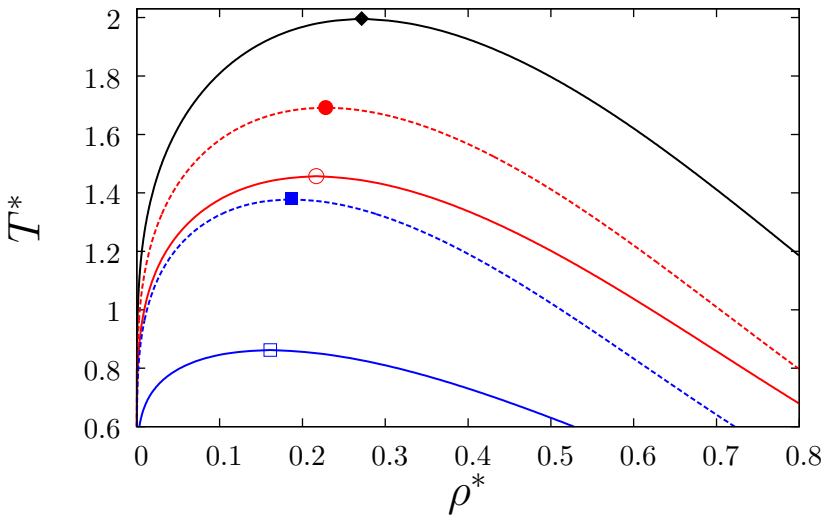

Figure 8: Liquid-gas phase diagram of the hard-sphere Morse liquid confined in disordered hard-sphere matrix ($\epsilon_{01}^{(M)} = 0$) with $\eta_0 = 0$ (solid black line and filled diamond), $\eta_0 = 0.1$ and $\tau = 1$ (solid red line and empty circle), $\eta_0 = 0.1$ and $\tau = 1/2$ (dashed red line and filled circle), $\eta_0 = 0.2$ and $\tau = 1$ (solid blue line and empty square), $\eta_0 = 0.2$ and $\tau = 1/2$ (dashed blue line and filled square. Symbols denote position of the critical point). Here $T^* = k_B T/\epsilon_{11}^{(M)}$ and $\rho^* = \rho_1 \sigma_1^3$.

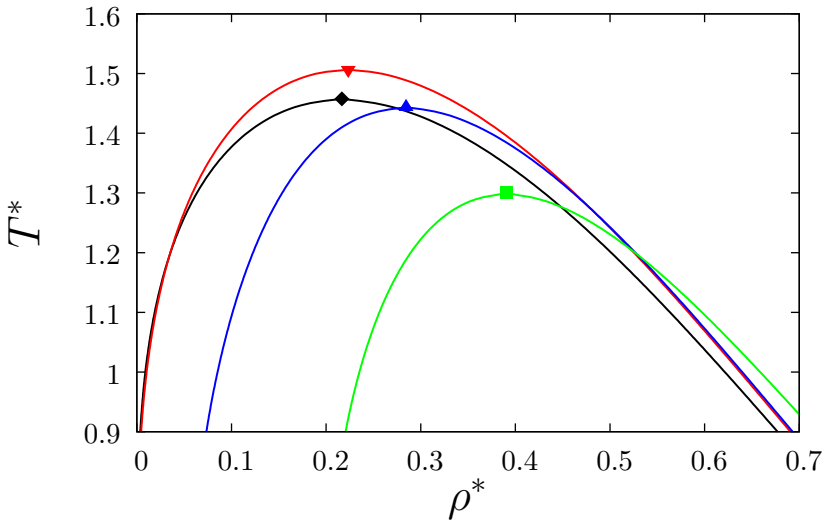

Figure 9: Liquid-gas phase diagram of the hard-sphere Morse liquid confined in disordered hard-sphere Morse matrix with $\eta_0 = 0.1$, $\tau = 1$ and $\epsilon_{01}^{(M)} = 0$ (black line and diamond), $\epsilon_{01}^{(M)}/\epsilon_{11}^{(M)} = 1$ (red line and downward triangle), $\epsilon_{01}^{(M)}/\epsilon_{11}^{(M)} = 3$ (blue line and upward triangle), $\epsilon_{01}^{(M)}/\epsilon_{11}^{(M)} = 6$ (green line and square). Here $T^* = k_B T/\epsilon_{11}^{(M)}$ and $\rho^* = \rho_1 \sigma_1^3$.

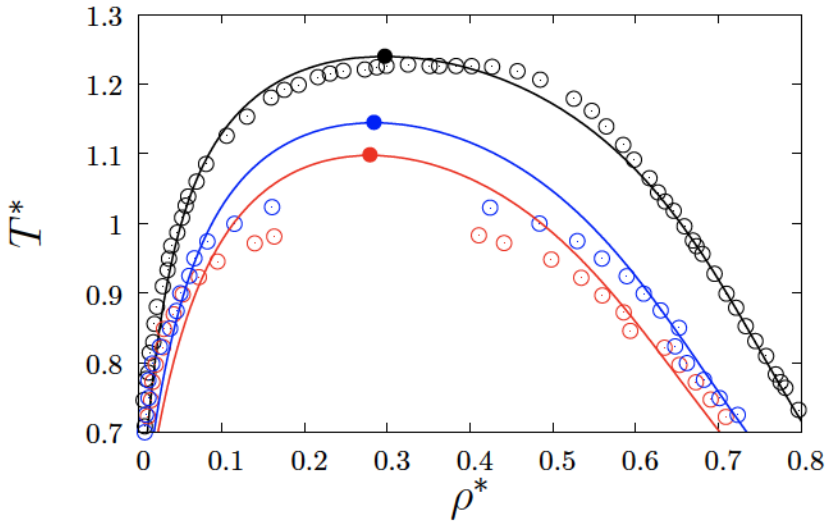

Figure 10: Liquid-gas phase diagram of the LJ liquid (18) in the bulk (black line and empty circles), confined in disordered hard-sphere matrix with $\eta_0 = 0.05$ and $\sigma_1^{(LJ)}/\sigma_0 = 1$ (red line and empty circles) and $\sigma_1^{(LJ)}/\sigma_0 = 2/3$ ((blue line and empty circles). Lines represent results of the theory, empty symbols denote computer simulation results [8] and filled symbols denote positions of the critical point. Here $T^* = k_B T/\epsilon_{11}^{(LJ)}$ and $\rho^* = \rho_1 \left(\sigma_1^{(LJ)}\right)^3 /(1 \quad \eta_0)$.

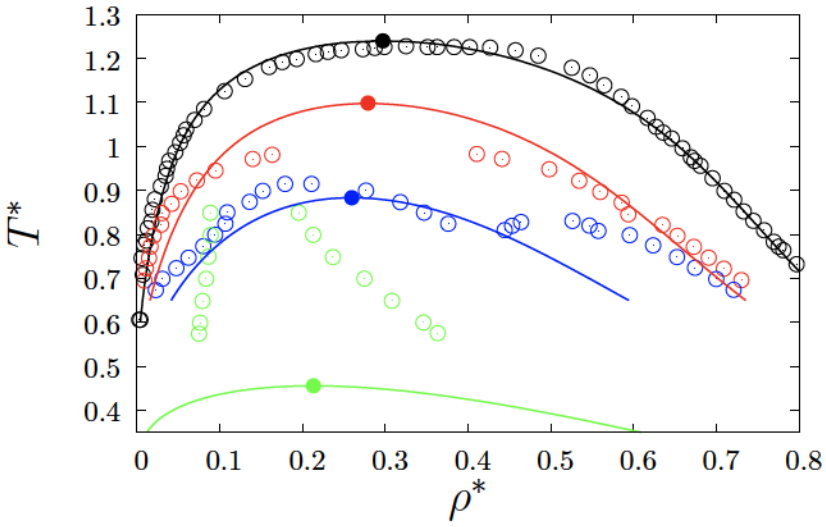

Figure 11: Liquid-gas phase diagram of the LJ liquid (18) in the bulk (black line and empty circles), confined in disordered hard-sphere matrix with $\sigma_1^{(LJ)}/\sigma_0 = 1$ and $\eta_0 = 0.05$ (red line and empty circles), $\eta_0 = 0.1$ (blue line and empty circles) and $\eta_0 = 0.2$ (green line and empty circles). Lines represent results of the theory, empty symbols denote computer simulation results [8] and filled symbols denote positions of the critical point. Here $T^* = k_B T/\epsilon_{11}^{(LJ)}$ and $\rho^* = \rho_1 \left(\sigma_1^{(LJ)}\right)^3 /(1 \quad \eta_0)$.

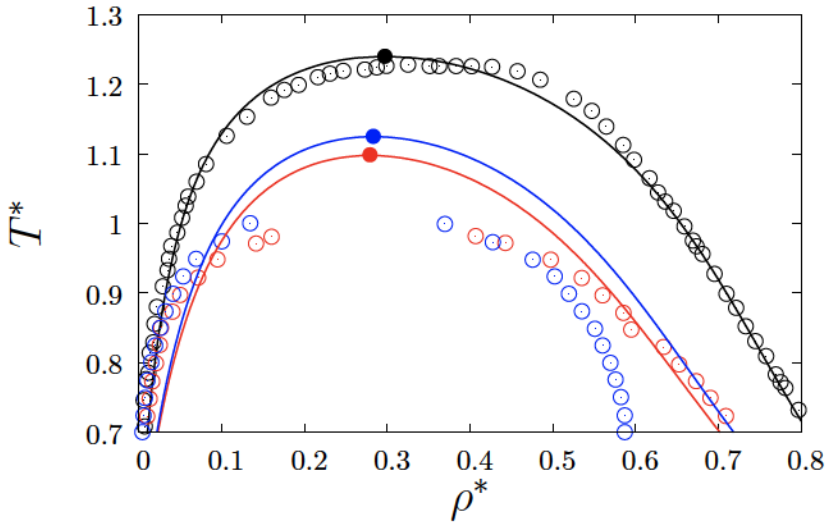

Figure 12: Liquid-gas phase diagram of the LJ liquid (18) in the bulk (black line and empty circles), confined in disordered hard-sphere matrix with $\eta_0 = 0.05$ and $\sigma_1^{(LJ)}/\sigma_0 = 1$ (blue line and empty circles), and confined in disordered LJ matrix with $\eta_0 = 0.05$, $\sigma_1^{(LJ)}/\sigma_0 = 1$ and $\epsilon_{01}^{(LJ)}/\epsilon_{11}^{(LJ)} = 1$ (red line and empty circles). Lines represent results of the theory, empty symbols denote computer simulation results [8] and filled symbols denote positions of the critical point. Here $T^* = k_B T/\epsilon_{11}^{(LJ)}$ and $\rho^* = \rho_1 \left(\sigma_1^{(LJ)}\right)^3 /(1 \quad \eta_0)$.

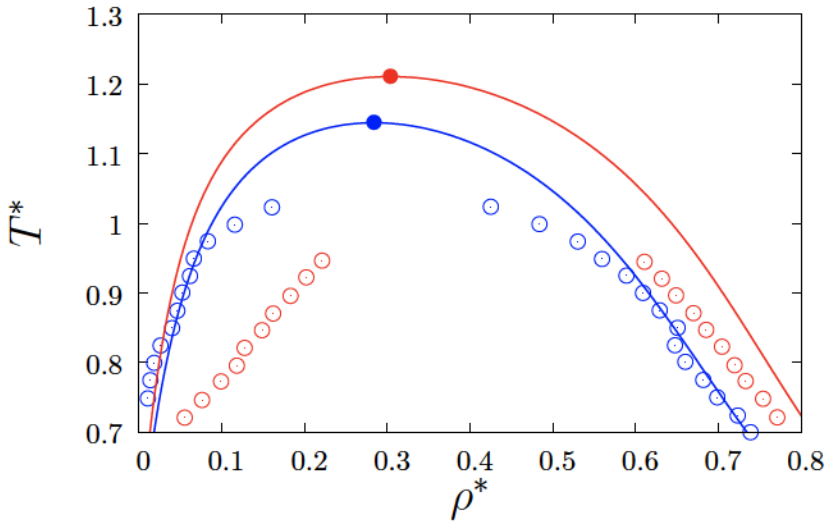

Figure 13: Liquid-gas phase diagram of the LJ liquid (18) confined in disordered hard-sphere matrix with $\eta_0 = 0.05$ and $\sigma_1^{(LJ)}/\sigma_0 = 3/2$ (blue line and empty circles) and confined in disordered LJ matrix with $\eta_0 = 0.05$, $\sigma_1^{(LJ)}/\sigma_0 = 3/2$ and $\epsilon_{01}^{(LJ)}/\epsilon_{11}^{(LJ)} = 1.25$ (red line and empty circles). Here $T^* = k_B T/\epsilon_{11}^{(LJ)}$ and $\rho^* = \rho_1 \left(\sigma_1^{(LJ)}\right)^3/(1 \quad \eta_0)$.

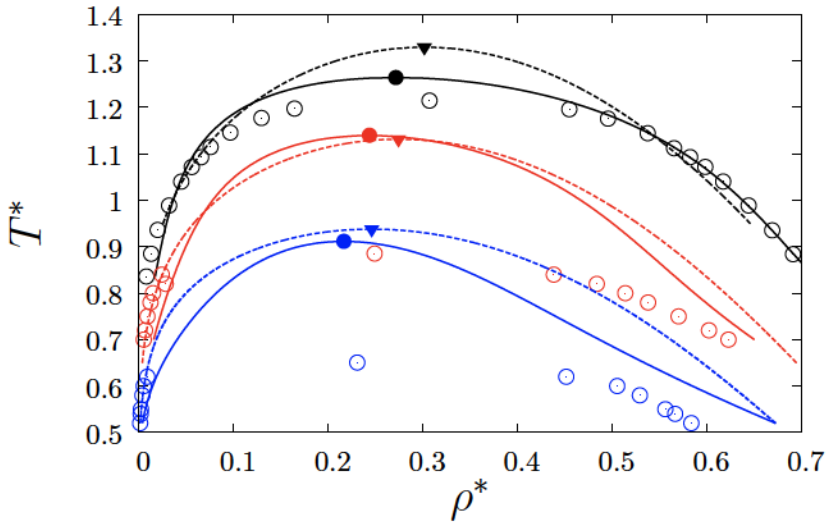

Figure 14: Liquid-gas phase diagram of hard-sphere SW liquid (19) in the bulk (black lines and empty circles), confined in disordered hard-sphere matrix with $\tau = 1$ and $\eta_0 = 0.05$ (red lines and empty circles), $\eta_0 = 0.1$ (blue lines and empty circles). Solid and dashed lines represent results of the present BH2 theory and the version of the BH2 theory of Hvozd et al. [44], empty circles stand for computer simulation results [53] and filled symbols denote position of the critical points. Here $T^* = k_B T/\epsilon_{11}^{(SW)}$ and $\rho^* = \rho_1 \sigma_1^3/(1 \quad \eta_0)$.

Appendix A. Fitting

The expression for the SW potential fit of $\epsilon_{11}^{(M)}$ is

$$\epsilon_{11}^{(M)}(T) = -1.4143(T^*)^3 + 3.6596(T^*)^2 - 2.8747(T^*) + 1.277. \qquad \text{(A1)}$$

where $T^* = k_B T/\epsilon_{11}^{(LJ)}$,

The expression for the LJ potential fit of $\epsilon_{11}^{(M)}$ is

$$\epsilon_{11}^{(M)}(T) = -0.6767(T^*)^3 + 1.5671(T^*)^2 - 0.9694(T^*) + 0.6733, \qquad \text{(A2)}$$

where $T^* = k_B T/\epsilon_{11}^{(SW)}$.